SARS-CoV-2 down-regulates ACE2 through lysosomal degradation

Yi Lu[a,†], Qingwei Zhu[a], Douglas M. Fox[a,b], Carol Gao[a], Sarah A. Stanley[a,b], and Kunxin Luo[a,*]
[a]Department of Molecular and Cell Biology, University of California, Berkeley, Berkeley, CA 94720; [b]Division of Infectious Diseases and Vaccinology, School of Public Health, University of California, Berkeley, Berkeley, CA 94720

ABSTRACT **Severe acute respiratory syndrome coronavirus 2 (SARS-CoV-2) utilizes its Spike (S) glycoprotein to bind to the angiotensin-converting enzyme 2 (ACE2) receptor for cellular entry. ACE2 is a critical negative regulator of the renin-angiotensin system and plays a protective role in preventing tissue injury. Expression of ACE2 has been shown to decrease upon infection by SARS-CoV. However, whether SARS-CoV-2 down-regulates ACE2 and the underlying mechanism and biological impact of this down-regulation have not been well defined. Here we show that the SARS-CoV-2 infection down-regulates ACE2 in vivo in an animal model, and in cultured cells in vitro, by inducing clathrin- and AP2-dependent endocytosis, leading to its degradation in the lysosome. SARS-CoV-2 S-treated cells and ACE2 knockdown cells exhibit similar alterations in downstream gene expression, with a pattern indicative of activated cytokine signaling that is associated with respiratory distress and inflammatory diseases often observed in COVID-19 patients. Finally, we have identified a soluble ACE2 fragment with a stronger binding to SARS-CoV-2 S that can efficiently block ACE2 down-regulation and viral infection. Thus, our study suggests that ACE2 down-regulation represents an important mechanism underlying SARS-CoV-2–associated pathology, and blocking this process could be a promising therapeutic strategy.**

Monitoring Editor
Mark Marsh
University College London

Received: Feb 14, 2022
Revised: Sep 30, 2022
Accepted: Oct 19, 2022

INTRODUCTION

Severe acute respiratory syndrome coronavirus 2 (SARS-CoV-2), the causal agent for the coronavirus disease 2019 (COVID-19), causes acute respiratory distress and long-term pulmonary damages as well as multiorgan dysfunctions involving cardiovascular, immune, gastrointestinal, and neurological systems (Finsterer *et al.*, 2021; Hu *et al.*, 2021; McCormick *et al.*, 2021). Similar to the original SARS-CoV virus, SARS-CoV-2 uses its Spike (S) glycoprotein on the envelope to engage the host cell surface angiotensin-converting enzyme 2 (ACE2) as the entry receptor, leading to the subsequent membrane fusion or endocytosis for virus entry (Li *et al.*, 2003; Hoffmann *et al.*, 2020; Ou *et al.*, 2020). Although the structure of the S-ACE2 complex and the mechanism by which ACE2 mediates viral entry have been elucidated (Lan *et al.*, 2020; Shang *et al.*, 2020; Wang *et al.*, 2020; Wrapp *et al.*, 2020; Yan *et al.*, 2020; Peng *et al.*, 2021; Jackson *et al.*, 2022), the impact of S protein on ACE2 expression and activity is not fully understood.

ACE2 is a type-I transmembrane carboxypeptidase that is expressed in multiple tissues, including lung, heart, blood vessels, kidney, and intestine (Hikmet *et al.*, 2020). It functions as a negative regulator of the renin-angiotensin system (RAS) by catalyzing the hydrolysis of angiotensin II, a peptide hormone that promotes vasoconstriction and increases blood pressure, into angiotensin 1–7 (Deshotels *et al.*, 2014; Santos *et al.*, 2018). ANG-(1–7) has been reported to reduce lung inflammation, fibrosis, and pulmonary arterial hypertension, likely through reducing the activity of key signaling pathways including the NF-κB, TGF-β, IL-6, IL-1β, JNK, and

This article was published online ahead of print in MBoC in Press (http://www.molbiolcell.org/cgi/doi/10.1091/mbc.E22-02-0045) on October 26, 2022.

†Present address: Tongji University Cancer Center, Shanghai Tenth People's Hospital, School of Medicine, Tongji University, Shanghai 20092, China.

*Address correspondence to: Kunxin Luo (kluo@berkeley.edu).

Abbreviations used: ACE2, angiotensin-converting enzyme 2; AIF, apoptosis inducing factor; ANG-(1–7), angiotensin 1–7; AP2, adaptor protein complex 2; CAV-1, caveolin-1; CHC, clathrin heavy chain; CHX, cycloheximide; CME, clathrin-mediated endocytosis; DAPI, 4′,6-Diamidino-2-phenylindole; EEA1, early endosome antigen 1; LAMP2, lysosomal-associated membrane protein 2; MDM2, murine double minute 2; PDI, protein disulfide isomerase; qRT-PCR, real-time quantitative reverse transcription PCR; RAB5, RAB5A, member RAS oncogene family; RAB7, RAB7A, member RAS oncogene family; RAS, renin-angiotensin system; RBD, receptor binding domain; RCAS1, receptor binding cancer antigen expressed on SiSo cells; S, spike protein; sACE2, soluble ACE2; SARS-CoV-2, severe acute respiratory syndrome coronavirus 2; SARS-CoV, severe acute respiratory syndrome coronavirus; siRNA, small interfering RNA; TCID50, median tissue culture infective dose; VSV-G, vesicular stomatitis virus glycoprotein.

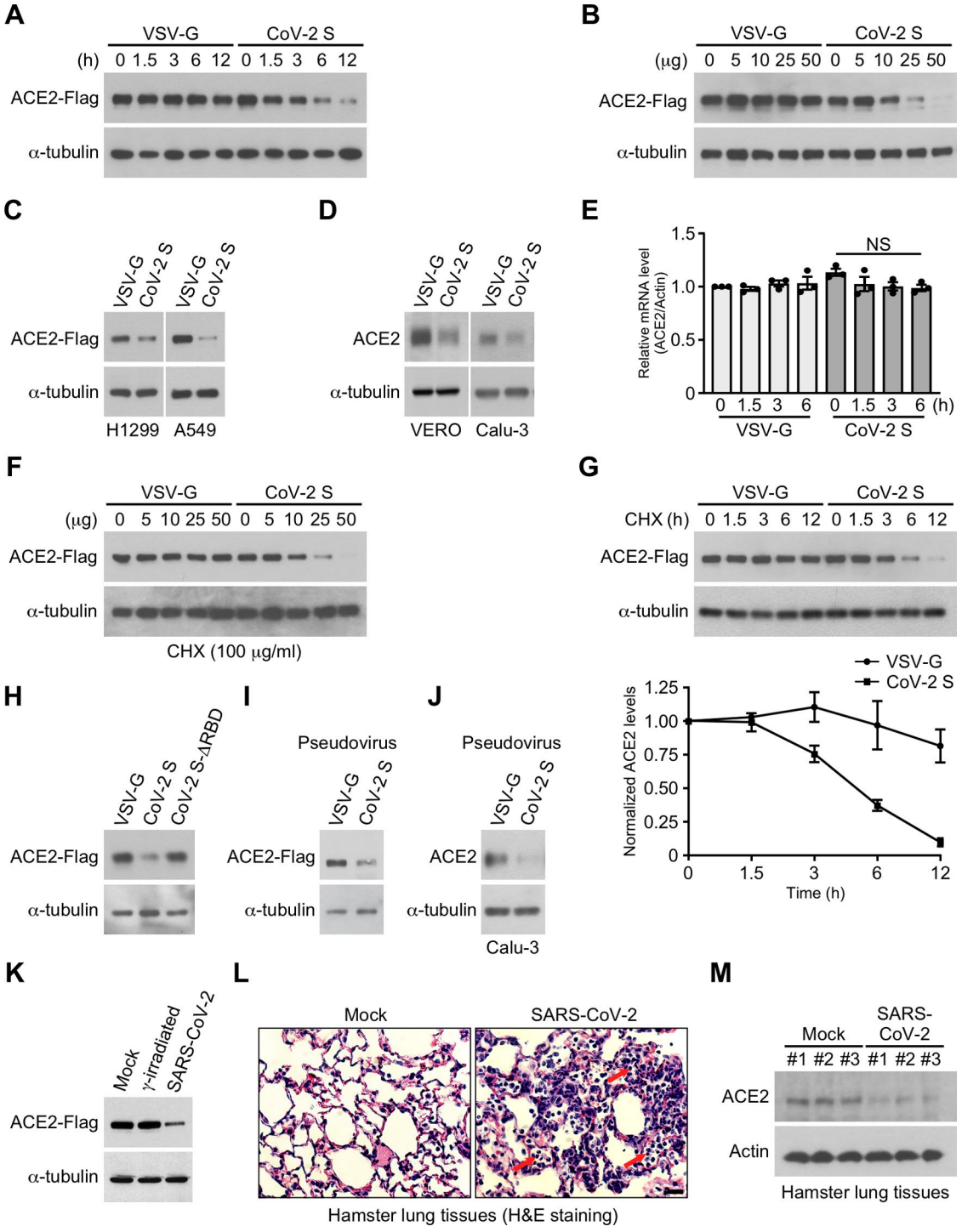

FIGURE 1: SARS-CoV-2 Spike protein down-regulates ACE2 both in vitro and in vivo. (A, B) CoV-2 S protein down-regulated ACE2 in HEK-293A^{ACE2} cells. HEK-293A^{ACE2} cells were treated with 25 μg of purified CoV-2 S or VSV-G for the indicated times (A) or with the indicated amount of CoV-2 S or VSV-G for 6 h (B) and subjected to Western blotting with anti-Flag. α-Tubulin was used as a loading control. (C) CoV-2 S decreased ACE2 in H1299^{ACE2} and A549^{ACE2} cells. Cells were treated with 25 μg of purified CoV-2 S or VSV-G for 6 h. (D) CoV-2 S decreased ACE2 in Vero and Calu-3 cells. Cells were treated with 25 μg of purified CoV-2 S or VSV-G for 6 h and subjected to Western blotting with anti-ACE2. (E) CoV-2 S did not alter ACE2 mRNA level as examined by RT-qPCR analysis in HEK-293A^{ACE2} cells treated with CoV-2 S or VSV-G. Data are mean ± SEM. Each dot represents the relative mRNA expression level of ACE2 in a single sample. *P* values were determined using unpaired two-tailed Student's *t* tests. NS, no significance. *n* = 3 independent experiments. (F, G) CoV-2 S promoted ACE2 degradation. HEK-293A^{ACE2} cells were treated with the indicated amount of CoV-2 S or VSV-G and 100 μg/ml cycloheximide (CHX) for 6 h (F) or with 25 μg CoV-2 S or VSV-G and 100 μg/ml CHX for the indicated time (G). ACE2 levels were measured by Western blotting with anti-Flag (top panel) and quantified in the graph shown in the bottom panel. Data are mean ± SEM. *n* = 3 independent experiments. (H) CoV-2 S RBD was required for ACE2 down-regulation. HEK-293A^{ACE2} cells were treated with 25 μg of CoV-2 S or CoV-2 S-ΔRBD for 6 h.

MAPK/ERK pathways (Santos *et al.*, 2018). Thus, ACE2 plays a protective role in preventing tissue injuries, and decreased expression of ACE2 is associated with an increase in pulmonary edema, acute respiratory distress syndrome, atherosclerosis, hypertension, cardiac hypertrophy, ventricular remodeling, and heart failure (Hamming *et al.*, 2007; Santos *et al.*, 2018; Vieira *et al.*, 2021). Consistently, ACE2 knockout mice exhibit increased susceptibility to cardiac injury and a worse outcome in various mouse models of inflammation and injury, such as influenza virus–induced lung injury and models of acute respiratory distress syndrome, among others (Imai *et al.*, 2010; Liu *et al.*, 2014; Jia *et al.*, 2020). For example, in response to acid challenge, ACE2 knockout mice displayed significantly greater lung elastance, worsened oxygenation, massive lung oedema, and increased inflammatory infiltration (Imai *et al.*, 2005, 2010). These phenotypes are very similar to those of mice that have been administered with SARS-CoV virus or the S protein of SARS-CoV (Kuba *et al.*, 2005). These SARS-CoV–infected mice showed worsened acid-induced acute lung failure accompanied by pathological changes in the lung parenchyma and increased lung edemas, leukocyte infiltration, and greater elastance. Importantly, ACE2 was found to be markedly reduced in the lungs of SARS-CoV–infected mice (Kuba *et al.*, 2005). Thus, ACE2 down-regulation may contribute to severe pathological outcomes upon SARS-CoV infection.

Multitissue injury, especially in the lung and cardiovascular system, is also an important feature of severe COVID-19 disease. Because the S protein of SARS-CoV-2 shares a high-level similarity with that of SARS-CoV and both bind to the ACE2 receptor (Li *et al.*, 2005; Wrapp *et al.*, 2020), we wonder whether infection with SARS-CoV-2 also leads to down-regulation of ACE2 and whether this contributes to the severe respiratory distress syndrome and dysfunctions in the cardiovascular system and other organs. In this study, we investigated whether SARS-CoV-2 triggers ACE2 down-regulation in vivo and in vitro and uncovered molecular mechanisms underlying this down-regulation. Using animal models of SARS-CoV-2 infection, a pseudovirus, and purified SARS-CoV-2 S protein, we showed that the SARS-CoV-2 S protein down-regulates ACE2 by inducing its endocytosis via clathrin and AP-2, leading to its degradation in the lysosome. A comparison of the alterations in gene expression between SARS-CoV-2 S–treated cells and ACE2-depleted cells showed a significant overlap between the two, suggesting that down-regulation of ACE2 may contribute to the pathological symptoms and altered cytokine and inflammatory signaling. Finally, we have identified a novel soluble ACE2 with a stronger binding to the SARS-CoV-2 S protein that could have therapeutic potentials. Thus, we have identified a potentially important mechanism for COVID-19 pathogenesis that may be exploited for developing effective therapeutics for COVID-19.

RESULTS

The S protein of SARS-CoV-2 down-regulates ACE2

To investigate the effect of SARS-CoV-2 S protein (CoV-2 S) on ACE2 levels, we first generated the HEK-293A^{ACE2} cell line that stably expressed Flag-tagged human ACE2 (ACE2-Flag) and then treated the cells with purified recombinant CoV-2 S protein (WA1 strain) or VSV glycoprotein (VSV-G) (Supplemental Figure S1A) for various periods of time. As shown in Figure 1, A and B, CoV-2 S, but not VSV-G, decreased ACE2 protein levels in a dose-dependent manner after 3 h. Similarly, CoV-2 S caused a decrease in ACE2 levels in two human lung cancer cell lines that stably expressed ACE2-Flag, H1299^{ACE2} and A549^{ACE2} (Figure 1C). More importantly, CoV-2 S decreased endogenous ACE2 levels in Vero and Calu-3 cells, two cell lines that are susceptible to infection by SARS-CoV-2 (Figure 1D) (Hoffmann *et al.*, 2020). Real-time quantitative reverse transcription PCR (qRT-PCR) analysis showed that the mRNA level of ACE2 was not altered upon CoV-2 S binding (Figure 1E), and down-regulation of ACE2 still occurred in the presence of the protein synthesis inhibitor cycloheximide (CHX) (Figure 1F). Furthermore, the half-life of ACE2 was greatly reduced upon S binding (Figure 1G), suggesting that CoV-2 S induces ACE2 degradation. Interestingly, deletion of the receptor binding domain (RBD) in CoV-2 S blocked the down-regulation of ACE2 (Figure 1H and Supplemental Figure S1B), suggesting that the interaction between the S protein and ACE2 is required for ACE2 down-regulation.

We next prepared the lentivirus-based pseudoviruses expressing either CoV-2 S or VSV-G to deliver the S protein to cells through viral infection. CoV-2 S and VSV-G were found to incorporate into the pseudoviruses (Supplemental Figure S1C), which subsequently infected cells in an ACE2-dependent manner (Supplemental Figure S1D). We then infected the HEK-293A^{ACE2} and Calu-3 cells and found that cells infected with viruses containing CoV-2 S, but not those expressing VSV-G, showed reduced ACE2 levels (Figure 1, I and J). Furthermore, the live SARS-CoV-2 virus, but not the inactivated, γ-irradiated SARS-CoV-2 virus, decreased ACE2 levels in HEK-293A^{ACE2} cells (Figure 1K). This suggests that CoV-2 S protein expressed from a live virus also leads to down-regulation of ACE2.

To investigate whether SARS-CoV-2 infection leads to down-regulation of endogenous ACE2 in vivo, we infected Syrian hamsters, an animal model commonly used for SARS-CoV-2 infection, with SARS-CoV-2 viruses intranasally (Hou *et al.*, 2020; Plante *et al.*, 2021). SARS-CoV-2 nucleocapsid protein could be observed in the infected cells of the lung tissues at day 2 postinfection, indicating that most of the infected cells at this early stage are still alive (Hou *et al.*, 2020; Yamaguchi *et al.*, 2021). Histopathological analysis revealed acute lung injury with increased infiltration of mononuclear cells in hamsters challenged with SARS-CoV-2 (Figure 1L). Notably, ACE2 levels in the lung tissues of these infected hamsters were significantly reduced at day 2 postinfection (Figure 1M), raising the possibility that reduced ACE2 expression might have a role in SARS-CoV-2–mediated lung pathologies. Taken together, our data suggest that SARS-CoV-2 infection down-regulates ACE2 in vivo and this is likely due to the binding of its S protein to ACE2 as purified S protein induces ACE2 degradation in vitro in cells.

(I, J) Pseudovirus bearing CoV-2 S down-regulated ACE2. HEK-293A^{ACE2} (I) or Calu-3 (J) cells were infected with pseudoviruses bearing CoV-2 S or VSV-G (MOI = 12) for 6 h and then subjected to Western blotting with anti-Flag (I) or anti–ACE-2 (J). (K) SARS-CoV-2 down-regulated ACE2 in cells. HEK-293A^{ACE2} cells were infected with SARS-CoV-2 or γ-irradiated SARS-CoV-2 (MOI = 12) for 6 h and then subjected to Western blotting with anti-Flag. (L) SARS-CoV-2 induced lung injury as indicated by the increased inflammatory infiltration. Representative H&E stains of lung tissues harvested from hamsters infected with SARS-CoV-2 or mock virus ($TCID^{50} = 4 \times 10^3$) at day 5 postinfection. Red arrows indicate the infiltrated mononuclear cells. $n = 3$ hamsters per group. Scale bar, 50 μm. (M) SARS-CoV-2 down-regulated ACE2 in vivo in infected lung tissues. SARS-CoV-2 or mock virus–infected hamster lung tissues were subjected to Western blotting analysis with anti-ACE2 antibody. $n = 3$ individual samples.

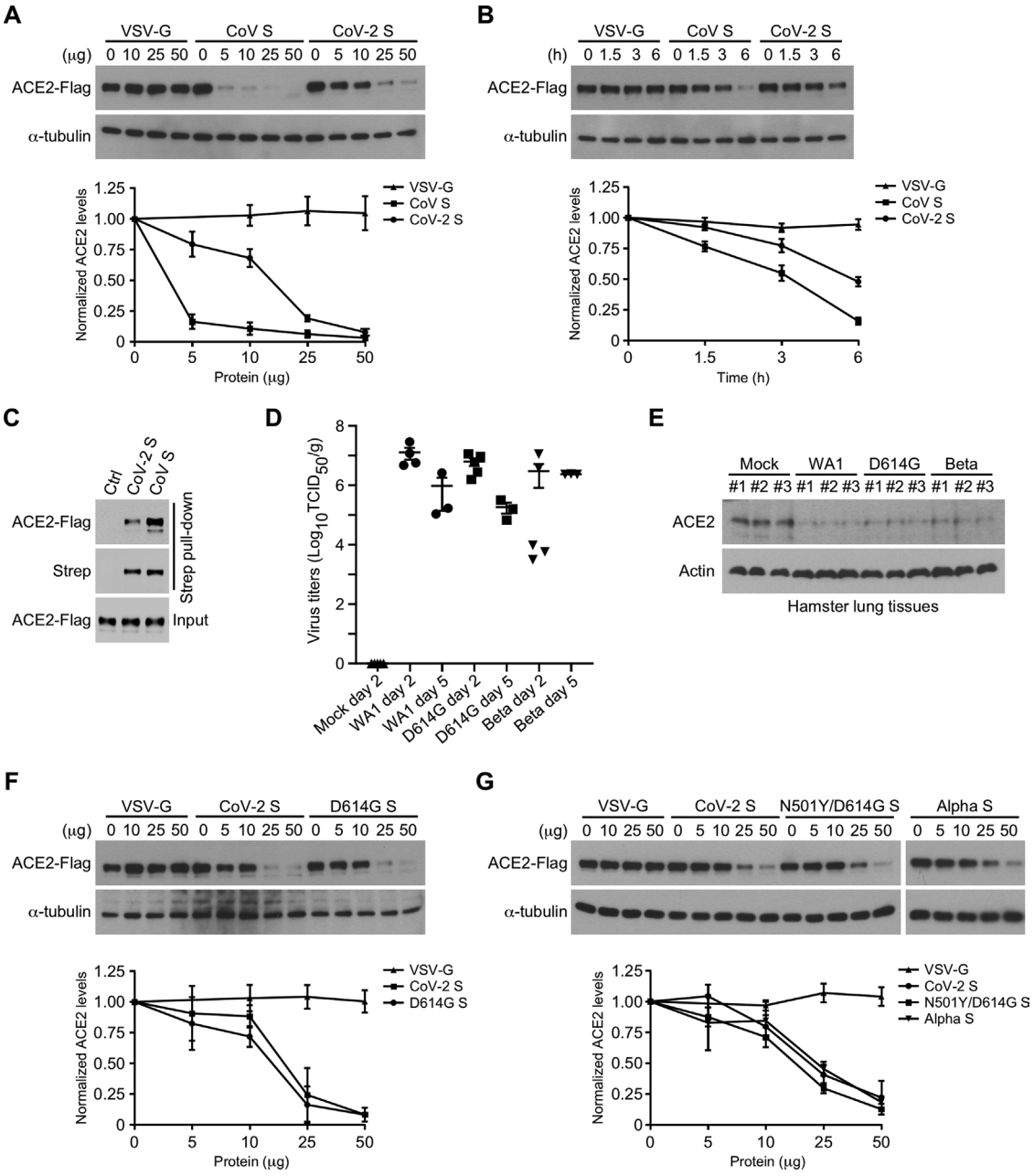

FIGURE 2: Down-regulation of ACE2 by the S protein of different SARS-CoV-2 strains. (A, B) CoV S down-regulated ACE2 more efficiently than CoV-2 S. HEK-293A^{ACE2} cells were treated with different amounts of VSV-G, CoV S, or CoV-2 S protein for 6 h (A) or with 17.5 μg of VSV-G, CoV S, or CoV-2 S protein for the indicated time (B) and then subjected to Western blotting analysis. ACE2 levels were quantified, normalized to that of α-tubulin, and are shown in the graphs. Data are mean ± SEM. $n = 3$ independent experiments. (C) Strep pull-down assay was performed by incubating purified Strep-tagged CoV S or CoV-2 S with lysates of HEK-293A^{ACE2} cells, and the associated ACE2 proteins were detected by Western blotting with anti-Flag. Strep-tagged S proteins were assessed by Western blotting with anti-Strep. ACE2 proteins in the cell lysates were examined by Western blotting with anti-Flag. (D) Titers of SARS-CoV-2 variants in the lungs of infected hamsters were determined on days 2 and 5 postinfection. Each hamster was infected with 4×10^3 TCID^{50} of virus. Each dot, square, or triangle represents the viral titer in each lung tissue of infected hamsters. Data are mean ± SD. $n = 3$, 4, or 5 hamsters per group. (E) SARS-CoV-2 variants down-regulated ACE2 in vivo in lung tissues. Lung tissues were harvested from SARS-CoV-2, SARS-CoV-2 variants, or mock virus–infected hamsters and subjected to Western blotting with anti-ACE2. $n = 3$ individual samples. (F, G) The S protein of CoV-2 variants down-regulated ACE2. HEK-293A^{ACE2} cells were treated with various amounts of S proteins from different variants for 6 h and then subjected to Western blotting with anti-Flag. ACE2 levels were quantified and normalized to that of α-tubulin and are shown in the graph. Data are mean ± SEM. $n = 3$ independent experiments.

Down-regulation of ACE2 by different S proteins

Because the Spike protein of the original SARS-CoV has been reported to down-regulate ACE2 (Kuba *et al.*, 2005; Haga *et al.*, 2008; Glowacka *et al.*, 2010), we next compared the efficiency of ACE2 down-regulation by the S proteins of SARS-CoV (CoV S) with that by CoV-2 S. The HEK-293A^{ACE2} cells were treated in parallel with the two S proteins at various concentrations and for different periods of time. Compared to CoV-2 S, a lower concentration of CoV S and a shorter time of treatment were sufficient to trigger ACE2 down-regulation (Figure 2, A and B, and Supplemental Figure S1E), suggesting that CoV S induced ACE2 down-regulation more efficiently than CoV-2 S. Given that the interaction between the S protein and ACE2 was required for ACE2 down-regulation, we employed a Strep pull-down assay to compare the binding ability of in vitro purified Strep-tagged CoV S for ACE2 with that of CoV-2 S. As shown in Figure 2C, CoV S displayed a stronger binding for ACE2 than CoV-2 S. This higher binding ability between CoV S and ACE2 could contribute to the increased efficiency in ACE2 degradation.

Several variants of SARS-CoV-2 carrying key point mutations in the S protein have emerged and circulated in the human population. These mutations include D614G, N501Y/D614G, N501Y/D614G/Δ69-70/P681H (Alpha), and N501Y/D614G/K417N/E484K (Beta) variants (Garcia-Beltran *et al.*, 2021; Harvey *et al.*, 2021; Li *et al.*, 2021; Martin *et al.*, 2021; Washington *et al.*, 2021; Zhou *et al.*, 2021). To determine whether these variants also trigger ACE2 down-regulation, we infected Syrian hamsters with similar titers of the SARS-CoV-2 viruses of the WA1, D614G, or Beta strains. At day 2 postinfection, hamsters infected with different variants exhibited similar viral titers in the lung, and by day 5, while the viral titers started to decrease in the lungs of hamsters infected with the WA1 and D614G strains, they maintained the same level in those infected with the Beta variant (Figure 2D). We harvested the lungs from the infected hamsters at day 2 and examined ACE2 levels by Western blotting. As shown in Figure 2E, all variants down-regulated ACE2 in lung tissues. Consistent with the in vivo results, purified S proteins containing the D614G, N501Y/D614G, or N501Y/D614G/Δ69-70/P681H (Alpha) mutations also down-regulated ACE2 in HEK-293A^{ACE2} cells as efficiently as the S protein from the original WA1 strain (Figure 2, F and G, and Supplemental Figure S1E). Taken together, our results indicate that the S proteins from the SARS-CoV and SARS-CoV-2 viruses induce ACE2 degradation both in vitro and in vivo.

The S protein down-regulates ACE2 through the lysosome

The proteasome and lysosome are two major routes of protein degradation (Perera and Zoncu, 2016; Dikic, 2017). To determine which of these two mediates ACE2 down-regulation, we pretreated cells with the proteasome inhibitor MG132 or the lysosome inhibitor bafilomycin A1 (Baf-A1) before adding the S protein. As shown in Figure 3, A and B, Baf-A1, but not MG132, prevented ACE2 down-regulation by CoV-2 S. Furthermore, specific lysosomal protease inhibitors E64d and pepstatin A also prevented CoV-2 S-induced ACE2 down-regulation (Supplemental Figure S2), suggesting the involvement of the lysosome in ACE2 down-regulation. Consistent with this, ACE2 that was normally localized to the cell membrane was internalized upon CoV-2 S binding, and the internalized ACE2 colocalized with the lysosome marker LAMP2, but not with markers of other organelles such as AIF (mitochondria) and RCAS1 (Golgi) (Figure 3, C–E). A previous report showed that ACE2 could be ubiquitinated by the MDM2 E3 ligase at K788, leading to its degradation (Shen *et al.*, 2020). We found that MDM2 is not involved in CoV-2 S-induced ACE2 down-regulation because knocking down of MDM2 or mutation of the K788 had no effect on ACE2 degradation (Figure 3, F and G). Thus, CoV-2 S protein down-regulates ACE2 via the lysosome pathway.

The SARS-CoV-2 S protein induces ACE2 endocytosis

Considering that endocytosis is the primary route for receptor internalization from the cell surface to the lysosome (Bonifacino and Traub, 2003), we next examined whether CoV-2 S promoted ACE2 endocytosis. We first generated the HEK-293A cell line stably expressing ACE2 fused to GFP and directly monitored the movement of ACE2-GFP by live-cell imaging. In untreated cells, ACE2-GFP was localized primarily at the cell surface (Figure 4A). Upon CoV-2 S binding, ACE2-GFP gradually translocated to cytoplasmic puncta and after 1 h had largely disappeared from the cell surface (Figure 4, A–C). The internalized ACE2-GFP colocalized with EEA1 and RAB5, two early endosome markers, and the late endosome marker RAB7, but not with markers of mitochondria (AIF), Golgi (RCAS1), endoplasmic reticulum (PDI), or autophagosome (LC3) (Figure 4, B–E). Interestingly, CoV-2 S colocalized with ACE2 both on the cell surface upon the initial binding and inside the cells after 3 h (Figure 4F), suggesting that the S protein was internalized together with ACE2. These results indicate that ACE2 undergoes endocytosis to the endosome upon CoV-2 S binding.

Clathrin and AP2 are required for CoV-2 S-induced ACE2 endocytosis

Given that the caveolae-dependent and clathrin-dependent pathways are two common endocytic pathways for receptor endocytosis (Mayor and Pagano, 2007; Mettlen *et al.*, 2018), we asked whether caveolae or clathrin was required for ACE2 endocytosis. To do this, we depleted the caveolin-1 (CAV-1) or clathrin heavy chain (CHC) by small interfering RNA (siRNA) in HEK-293A^{ACE2} cells (Figure 5, A–C) and found that knockdown of CHC, but not CAV-1, prevented ACE2 down-regulation and endocytosis by CoV-2 S, suggesting that ACE2 likely underwent clathrin-mediated endocytosis (CME).

CME is a complex and multistep process that removes transmembrane proteins from the plasma membrane. Adaptor protein complex 2 (AP2) recognizes and binds to the sorting signals on the intracellular domains of transmembrane cargo proteins to internalize them through endocytosis (Kaksonen and Roux, 2018). To investigate the role of AP2 in ACE2 down-regulation, we knocked down the μ2 subunit of AP2 by siRNA and found that depletion of μ2 suppressed ACE2 down-regulation (Figure 5D) and internalization (Figure 5E). These results suggest that AP2 is required for S protein–mediated ACE2 degradation. Consistent with this, μ2 was found to colocalize with ACE2 and the S protein (Figure 5F).

ACE2, in its cytoplasmic tail region, contains a YASI sequence, which is a putative endocytic sorting motif (YxxΦ, in which x is any amino acid and Φ represents amino acids with a bulky hydrophobic side chain) and is predicted to bind to the μ2 subunit of the endocytosis AP2 complex (Figure 5G). To test whether AP2 binds to the ACE2 YASI motif, we first mutated this motif to AASA and confirmed that CoV-2 S could still interact with the ACE2-AASA mutant (Supplemental Figure S3). We then purified AP2 complex from 293T cells transfected with cDNAs encoding various tagged AP2 subunits, including μ2, Strep-α, mCherry-β2, and HA-σ2, and investigated the interaction between AP2 and ACE2 using a Strep pull-down assay. As shown in Figure 5H, the AP2 complex could bind to wild-type (WT) ACE2, but not the ACE2-AASA mutant, confirming that the YASI motif in ACE2 mediates binding to AP2. Consistent with this, CoV-2 S effectively caused down-regulation and internalization of WT ACE2 but not ACE2-AASA (Figure 5, I and J). Taken together, these data suggest that the AP2 complex directly binds to ACE2 to facilitate its CME, ultimately resulting in lysosomal degradation.

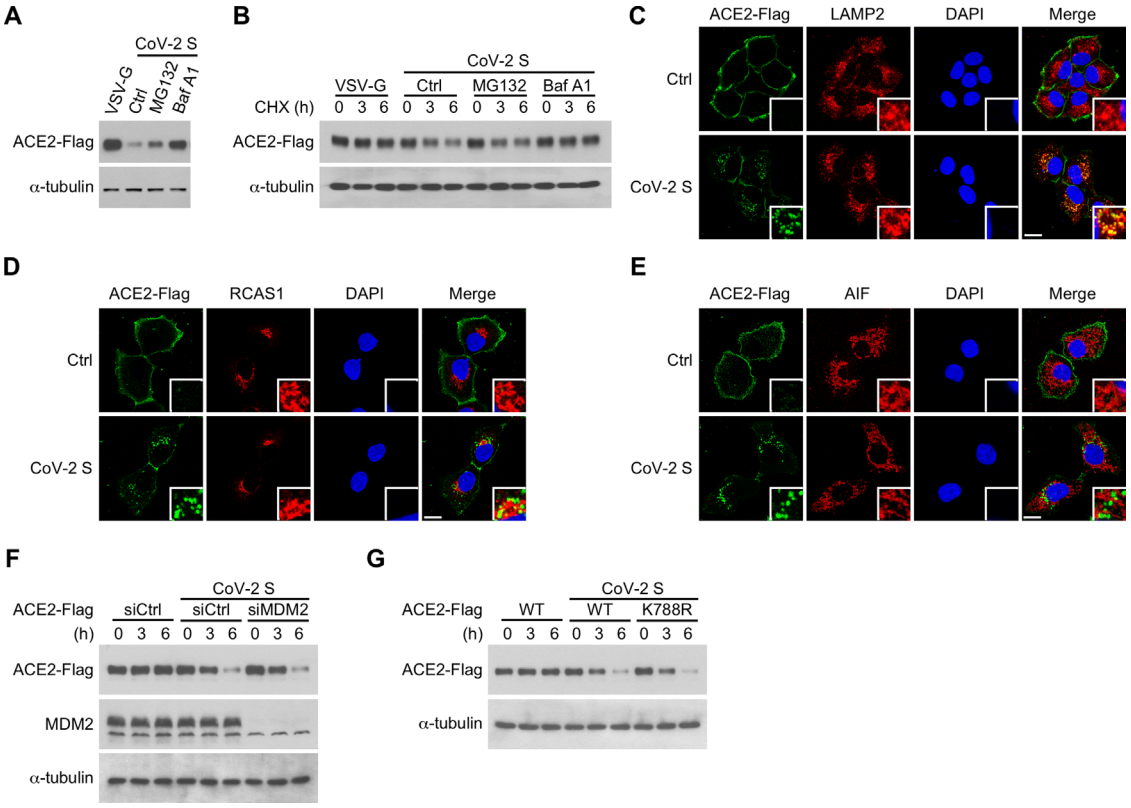

FIGURE 3: The CoV-2 S protein down-regulates ACE2 through the lysosome. (A, B) CoV-2 S down-regulated ACE2 through the lysosome. HEK-293A^{ACE2} cells were pretreated with 10 μM proteasome inhibitor MG132 or 200 nM lysosome inhibitor bafilomycin A1 (Baf A1) for 2 h, followed by 25 μg of CoV-2 S treatment for 6 h in the absence (A) or presence (B) of 100 μg/ml CHX for the indicated time. Levels of ACE2 were examined by Western blotting. (C–E) ACE2 was internalized and colocalized with lysosome markers upon CoV-2 S treatment. HEK-293A^{ACE2} cells were treated with CoV-2 S for 4 h and subjected to immunostaining with anti-ACE2 (green) and anti-LAMP2 (C), anti-RCAS1 (D), or anti-AIF (E) antibodies (red). DAPI is shown in blue. Scale bar, 10 μm. (F) MDM2 was not involved in CoV-2 S-mediated ACE2 down-regulation. HEK-293A^{ACE2} cells were transfected with siMDM2 or control (siCtrl) for 48 h and then treated with 25 μg of CoV-2 S protein for the indicated time. (G) HEK-293A cells stably expressing ACE2 or ACE2-K788R were treated with 25 μg of CoV-2 S protein for the indicated time, and ACE2 levels were measured by Western blotting.

Downstream transcription outcomes of CoV-2 S-induced ACE2 down-regulation

To investigate the downstream outcomes of CoV-2 S-induced ACE2 down-regulation, we first performed RNA-seq analysis in HEK-293A^{ACE2} cells treated with 25 μg of CoV-2 S for 6 h (Supplemental Figure S4). Analysis of the RNA-seq data revealed that 286 genes were up-regulated and 261 genes were down-regulated in CoV-2 S-treated cells (Figure 6A). DisGeNET analyses of these up-regulated genes showed significant enrichment of genes associated with pneumonia, respiratory distress syndrome, and lung diseases, pathological conditions often found in patients exhibiting severe symptoms following SARS-CoV-2 infection (Figure 6B). KEGG enrichment analysis further showed that genes associated with multiple signaling pathways, including MAPK, interleukin, cytokine, Hippo, and JAK-STAT pathways, were significantly enriched in the up-regulated gene set (Figure 6C).

Next, we compared this RNA-seq data set with that found in cells depleted of ACE2 (Supplemental Figure S4). Knocking down of ACE2 by siRNA (siACE2) resulted in the up-regulation of the expression of 539 genes and the down-regulation of 785 genes (Figure 6D). Many of these up-regulated genes are active in multiple cytokine signaling pathways and are related to arthritis, inflammation, cardiovascular diseases, and pneumonia (Figure 6, E and F), similar to that found in CoV-2 S-treated cells. In agreement with this, Venn diagram analysis showed an overlap of 187 genes between the CoV-2 S-treated cells and siACE2 cells (Figure 6G). Importantly, heat maps and DisGeNET analyses of these overlapped up-regulated genes also showed significant enrichment of genes that are associated with lung diseases, including asthma, pulmonary fibrosis, and pulmonary emphysema (Figure 6, H and I). Pathway analysis further revealed that many of these overlapped genes were concentrated in interleukin and cytokine signaling, JAK-STAT signaling, MAPK signaling, and the AP-1 transcription factor network, suggesting that ACE2 down-regulation may activate these signaling cascades (Figure 6J). Taken together, these data suggest that binding of CoV-2 S alone is sufficient to alter the activities of key pathways associated with SARS-CoV-2 pathogenesis and that some of the severe symptoms may be caused by ACE2 down-regulation (Bouhaddou *et al.*, 2020; Jiang *et al.*, 2020; Winkler *et al.*, 2020).

A soluble ACE2 fragment with a stronger binding to CoV-2 S blocks the binding and down-regulation of endogenous ACE2 by CoV-2 S

Structural studies have indicated that residues 31, 35, 38, and 353 in human ACE2 are the key binding sites for the SARS-CoV S protein (Lan *et al.*, 2020; Shang *et al.*, 2020; Walls *et al.*, 2020; Wang *et al.*, 2020; Wrapp *et al.*, 2020; Yan *et al.*, 2020). Among these, E35 and K353 are absolutely conserved among ACE2 from different species,

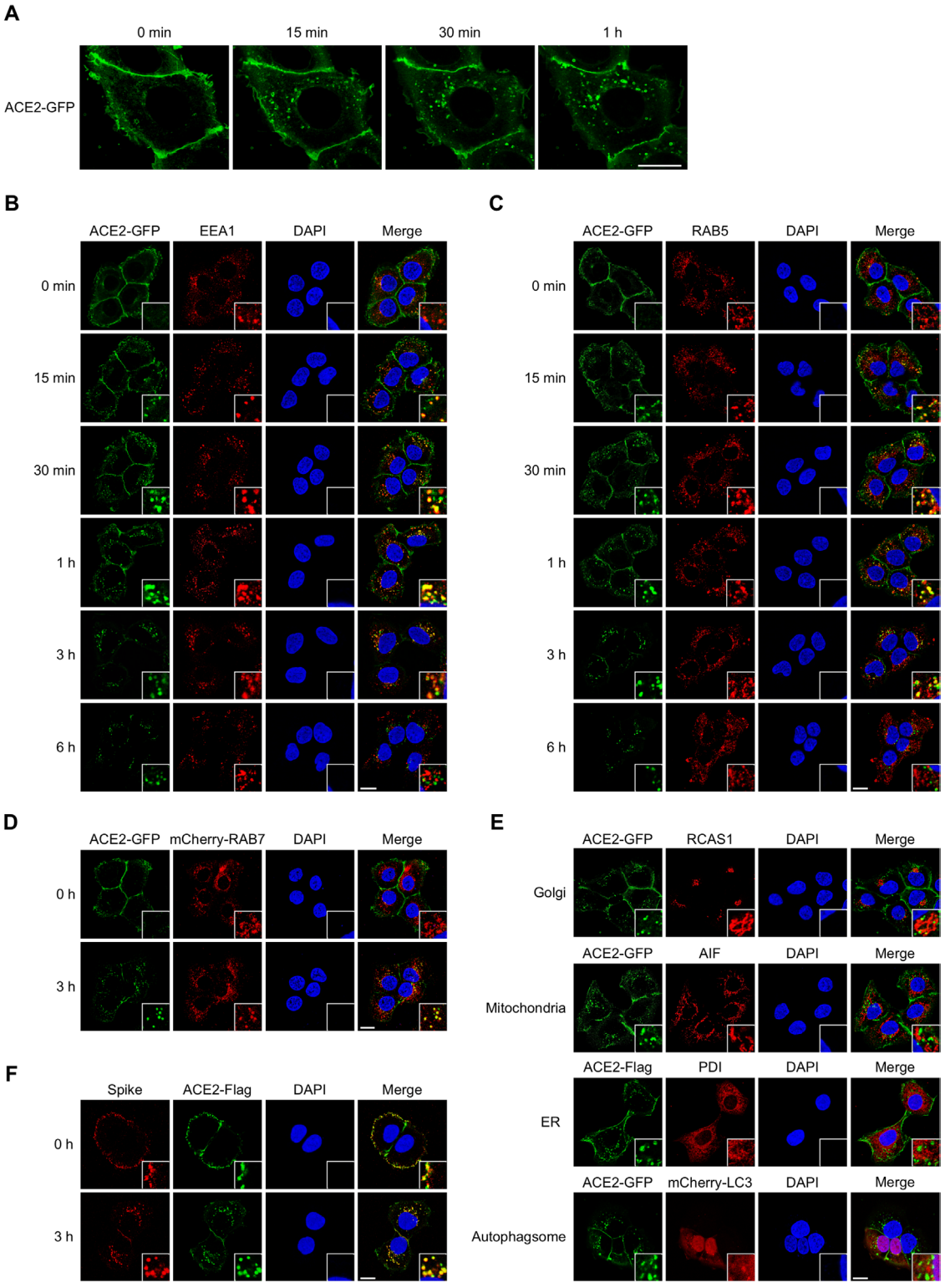

FIGURE 4: CoV-2 S induces ACE2 endocytosis. (A) ACE2 was internalized upon CoV-2 S treatment. HEK-293A cells stably expressing ACE2-GFP were treated with CoV-2 S and subjected to live-cell imaging. The durations of CoV-2 S treatment are indicated at the top. Scale bar, 10 μm. (B, C) ACE2 colocalized with early endosome markers. HEK-293A cells stably expressing ACE2-GFP were treated with CoV-2 S for the indicated time and subjected to immunostaining with anti-EEA1 (red) (B) or anti-RAB5 (red) (C) antibodies. DAPI is shown in blue. Scale bar, 10 μm. (D) ACE2 colocalized with a late endosome marker. HEK-293A cells stably expressing ACE2-GFP and mCherry-RAB7 were treated with CoV-2 S for 3 h and subjected to confocal microscopy. DAPI is shown in blue. Scale bar, 10 μm. (E) HEK-293A cells stably expressing ACE2-GFP or ACE2-Flag were treated with CoV-2 S for 3 h and subjected to immunostaining with anti-RCAS1 (red), anti-AIF (red), anti-PDI (red), or anti-ACE2 (green) antibodies. DAPI is shown in blue. Scale bar, 10 μm. (F) ACE2 colocalized with CoV-2 S. HEK-293A^{ACE2} cells were treated with CoV-2 S for 3 h and subjected to immunostaining with anti-ACE2 (green) and anti-Spike (red) antibodies. DAPI is shown in blue. Scale bar, 10 μm.

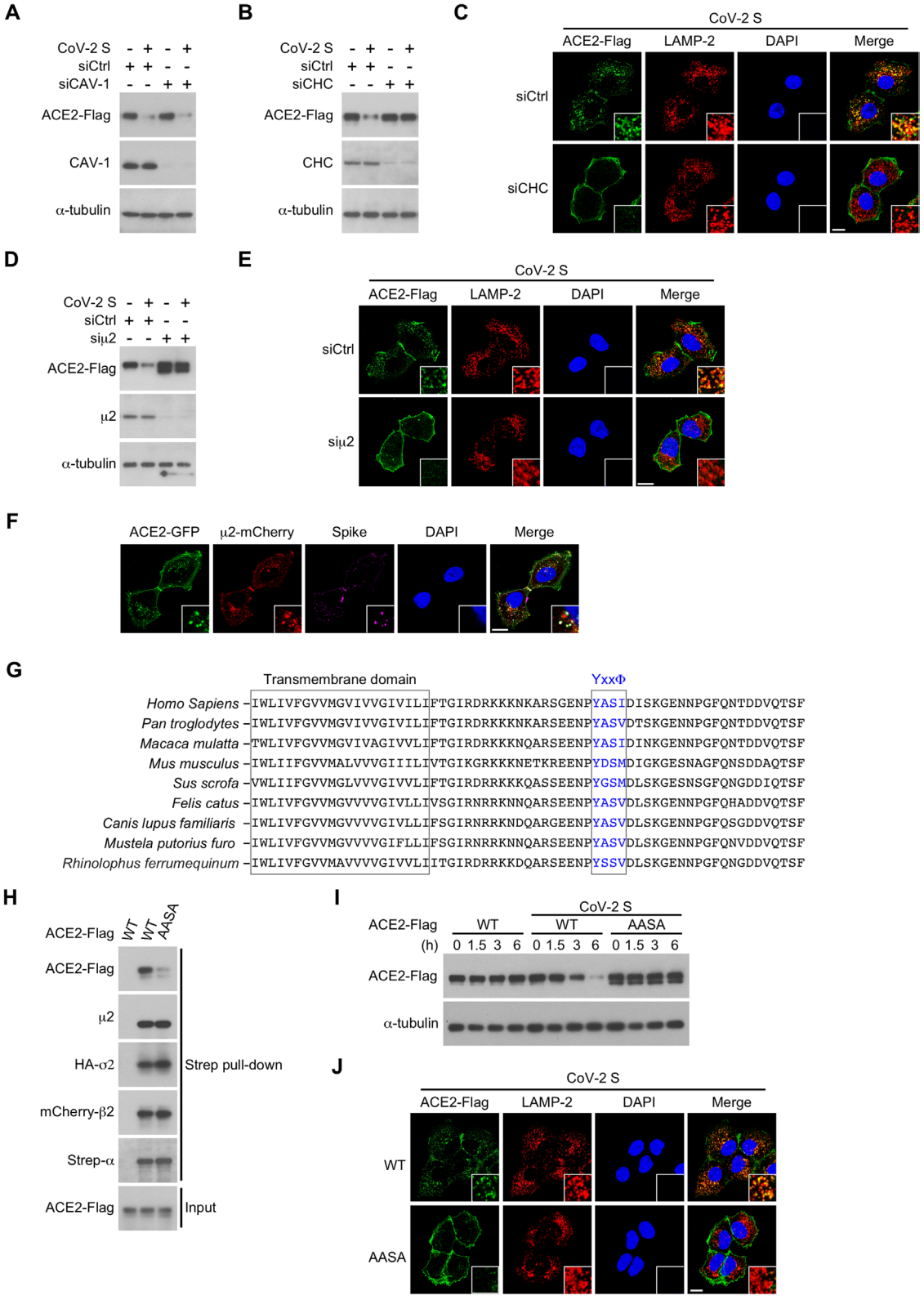

FIGURE 5: Clathrin and AP2 are required for SARS-CoV-2 S-induced ACE2 endocytosis. (A, B) Clathrin was required for ACE2 down-regulation. HEK-293A^{ACE2} cells were transfected with siCAV-1, siCHC, or siCtrl for 48 h and then treated with CoV-2 S protein for 6 h. Cell lysates were subjected to Western blotting with anti-Flag, anti-CAV-1, or anti-CHC antibodies. (C) Clathrin was required for ACE2 internalization. HEK-293A^{ACE2} cells were transfected with siCHC or siCtrl for 48 h, treated with CoV-2 S protein for 4 h, and then subjected to immunostaining with anti-ACE2 (green) and anti-LAMP2 (red) antibodies. DAPI is in blue. Scale bar, 10 μm. (D) μ2 was required for ACE2 down-regulation. HEK-293A^{ACE2} cells were transfected with siμ2 or siCtrl for 48 h and then treated with CoV-2 S protein for 6 h. Cell lysates were subjected to Western blotting analysis with anti-Flag and anti-μ2 antibodies. (E) μ2 was required for ACE2

while K31 and D38 in the ACE2 peptidase (PD) domain could potentially be altered to increase its binding to the S proteins. In particular, D38 normally forms a salt bridge with K353, a feature critical for the stabilization of the structure, and moreover, the civet ACE2 has an E at this position, with a longer side chain to form a stronger salt bridge. Thus, we speculate that a change of D38 to E in human ACE2 may increase its interaction with the S protein.

To test this, we changed K31 to T or D38 to E individually in human ACE2 and tested the binding of these mutants to CoV-2 S by a coimmunoprecipitation assay in 293T cells cotransfected with the CoV-2 S and WT or mutant ACE2. While K31T ACE2 significantly disrupted its binding to CoV-2 S (unpublished data), D38E mutation enhanced the binding of ACE2 to CoV-2 S (Figure 7A). Thus we decided to focus on the D38E ACE2.

Next we engineered a soluble D38E ACE2 fragment (1–615 amino acids) with its transmembrane and cytoplasmic domains removed (sACE2-D38E) and tested whether this soluble ACE2 could compete with the cellular ACE2 for binding to CoV-2 S. Indeed, the sACE2-D38E fragment competed with the full-length WT ACE2 in cells for binding to CoV-2 S in a dose-dependent manner (Figure 7B). Furthermore, addition of sACE2-D38E into the cell culture medium successfully blocked the ACE2 down-regulation caused by CoV-2 S (Figure 7C).

We also examined the binding ability of sACE2-D38E fragment for the S proteins of WT or the Alpha CoV-2 variant. As shown in Figure 7D, the sACE2-D38E fragment bound to Alpha CoV-2 S as efficiently as WT CoV-2 S.

Finally, to examine whether sACE2-D38E can prevent CoV-2 S-mediated viral entry into cells, a pseudovirus expressing both a luciferase reporter gene and the S protein from the WT SARS-CoV-2 strain or the Alpha variant was employed to infect HEK293A^{ACE2} cells in the absence or presence of sACE2-D38E. The level of viral entry into cells was measured by the luciferase assay (Hoffmann *et al.*, 2020). As shown in Figure 7E, 14 h after viral infection, the infected cells all displayed a significantly increased luciferase activity (top panels), indicating efficient viral entry. As expected, ACE2 was degraded significantly in these infected cells (bottom panels, Figure 7E). Addition of sACE2-D38E markedly suppressed luciferase activities and viral entry upon infection by both WT and Alpha strains of pseudovirus and blocked ACE2 down-regulation (Figure 7E). sACE2-D38E did not affect VSV-G–mediated viral infection, suggesting that sACE2-D38E specifically blocks CoV-2 S (Figure 7E). These data demonstrated that soluble ACE2 with a stronger binding to CoV-2 S can compete with cellular ACE2 to neutralize CoV-2 S-mediated viral infection and block the down-regulation of host ACE2, therefore preventing pathological symptoms associated with ACE2 down-regulation.

Taking the results together, our study has demonstrated that SARS-CoV-2 infection leads to down-regulation and degradation of ACE2 in vivo and provided important insights toward an understanding of the molecular mechanisms underlying the pathogenesis of SARS-CoV-2 infection.

DISCUSSION

Patients with severe COVID-19 display acute respiratory distress syndrome and multiorgan dysfunctions (Santos *et al.*, 2018). These symptoms are similar to the phenotypes observed in several tissue injury models of ACE2 knockout mice. This prompted us to examine whether SARS-CoV-2 infection or binding of the S protein causes down-regulation of ACE2 and whether this contributes to the observed pathological effects of SARS-CoV-2 infection. Using animal models of SARS-CoV2 infection, a pseudovirus and purified SARS-CoV-2 S protein, we showed that SARS-CoV-2 infection led to ACE2 down-regulation in vivo, and its S protein down-regulated ACE2 by inducing clathrin- and AP2-dependent endocytosis, leading to its degradation in the lysosome. CoV-2 S induces changes in downstream gene expression that are associated with respiratory and inflammatory diseases and affect cytokine signaling. Importantly, many of these changes are also observed in ACE2 knockdown cells, especially those related to pulmonary and inflammatory diseases and enriched in cytokine signaling pathways, suggesting that some of the severe respiratory and inflammatory symptoms exhibited by patients with severe COVID-19 can be attributed to ACE2 down-regulation. Thus, blocking the binding of the S protein to ACE2 and the subsequent down-regulation of ACE2 could lessen the tissue injury and severity of clinical symptoms. To that end, we have identified a soluble sACE2 fragment that displays a stronger binding to CoV-2 S that can efficiently block ACE2 down-regulation and CoV-2 pseudoviral infection. Taken together, our results suggest that ACE2 down-regulation represents an important mechanism for CoV-2–associated clinical pathological outcomes, and blocking this process could be a potential strategy for clinical therapy.

ACE2 plays a protective role in preventing multiple tissue injury, and down-regulation of ACE2 has been reported to occur during the development of pulmonary arterial hypertension (Shen *et al.*, 2020). This down-regulation appeared to be mediated by the proteasome and required the MDM2 E3 ubiquitin ligase, which induced ubiquitination of ACE2 at K788, targeting it for proteasome degradation (Shen *et al.*, 2020). However, MDM2 is not involved in CoV-2 S-induced ACE2 degradation, as depletion of MDM2 or mutation of K788R in ACE2 did not affect ACE2 down-regulation by CoV-2 S. In contrast, our results showed that CoV-2 S-induced ACE2 down-regulation occurs through the lysosome

internalization. HEK-293A^{ACE2} cells were transfected with siμ2 or siCtrl, treated with CoV-2 S protein for 4 h, and then subjected to immunostaining with anti-ACE2 (green) and anti-LAMP2 (red). DAPIis in blue. Scale bar, 10 μm. (F) ACE2 colocalized with μ2. HEK-293A cells stably expressing ACE2-GFP and μ2-mCherry were treated with CoV-2 S for 1 h and then subjected to immunostaining with anti-Spike (magenta) antibody. DAPI is shown in blue. Scale bar, 10 μm. (G) Sequence alignment of the transmembrane domain and cytoplasmic tail of ACE2 from different species. The YxxΦ motif is indicated in blue. (H) ACE2 interacted with the AP2 complex through the YASI motif. Purified Strep-tagged AP2 complex was incubated with lysates of cells stably expressing ACE2 or ACE2-AASA mutant, and the ACE2 associated with AP2 was detected by Western blotting with anti-Flag. Strep-tagged AP2 complex was assessed by Western blotting with anti-Strep, anti-mCherry, anti-HA, and anti-μ2. ACE2 proteins in the cell lysates were examined by Western blotting with anti-Flag. (I) The ACE2-AASA mutant was not down-regulated by CoV-2 S. HEK-293A cells stably expressing ACE2 or ACE2-AASA were treated with CoV-2 S for the indicated time and then subjected to Western blotting with anti-Flag. (J) The ACE2-AASA mutant was not internalized by CoV-2 S. HEK-293A cells stably expressing ACE2 or ACE2-AASA were treated with CoV-2 S for 4 h and then subjected to immunostaining with anti-ACE2 (green) and anti-LAPM2 (red) antibodies. DAPI is shown in blue. Scale bar, 10 μm.

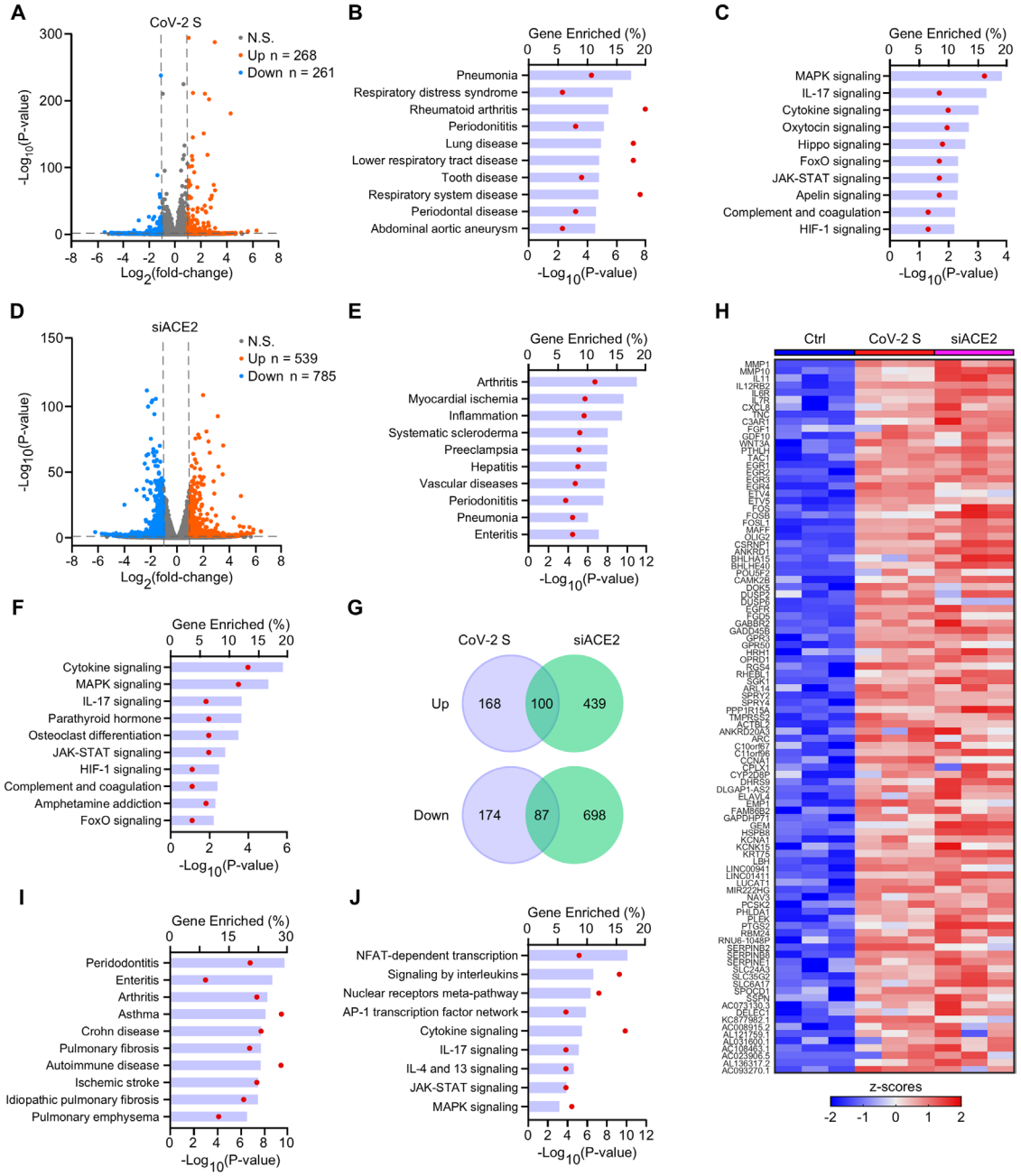

FIGURE 6: Effect of ACE2 down-regulation by CoV-2 S on downstream transcription responses. (A) Volcano plot showing differentially expressed genes in cells treated with CoV-2 S by RNA-seq. Each dot represents the average value of a single gene in three replicate experiments. Dashed horizontal lines mark a *P* value of 0.05, and dashed vertical lines indicate a Log2(fold change) of 1 and –1. Red and blue indicate up-regulated and down-regulated genes, respectively, with an absolute Log2(fold change) > 1 and a *P* value < 0.05. (B) DisGeNET enrichment analysis of CoV-2 S-induced up-regulated genes. Bars show the –Log10(*P* value). Red points show the percentage of genes enriched. (C) KEGG pathway enrichment analysis of CoV-2–induced up-regulated genes. Bars show the –Log10(*P* value). Red points show the percentage of genes enriched. (D) Volcano plot showing differentially expressed genes in ACE2 knockdown cells using RNA-seq. (E) DisGeNET enrichment analysis of up-regulated genes in ACE2 knockdown cells. Bars show the –Log10(*P* value). Red points show the percentage of genes enriched. (F) KEGG pathway enrichment analysis of up-regulated genes in ACE2 knockdown cells. Bars show the –Log10(*P* value). Red points show the percentage of genes enriched. (G) Venn diagram of overlapping up- or down-regulated genes identified in differential expression analysis of CoV-2 S-treated or ACE2 knockdown cells. Numbers of up-regulated or down-regulated genes in each group are indicated. (H) Heat maps of overlapping up-regulated genes in both CoV-2 S and ACE2 knockdown cells. Columns represent samples, and rows represent genes. Gene expression levels in the heat maps are z score–normalized Log2(CPM)-transformed values. CPM, count per million reads. (I) DisGeNET enrichment analysis of overlapped up-regulated genes in both CoV-2 S and ACE2 knockdown cells. Bars show the –Log10(*P* value). Red points show the percentage of genes enriched. (J) KEGG pathway enrichment analysis of overlapped up-regulated genes in both CoV-2 S and ACE2 knockdown cells. Bars show the –Log10(*P* value). Red points show the percentage of genes enriched.

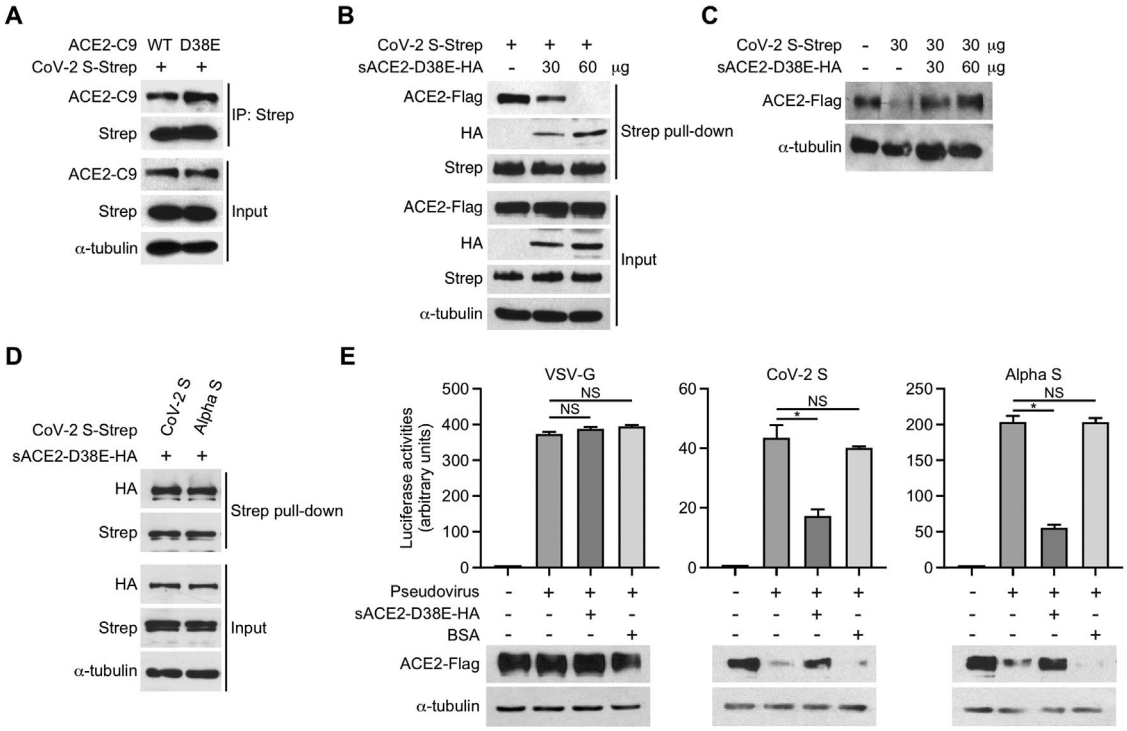

FIGURE 7: Identification of a soluble ACE2 fragment with a stronger binding to CoV-2 S. (A) The D38E mutation of ACE2 enhanced its binding to CoV-2 S. Strep-tagged CoV-2 S (CoV-2 S-Strep) was cotransfected with C9-tagged wild type (WT) or D38E mutant of ACE2 into 293T cells. Coimmunoprecipitation (co-IP) was performed with anti-Strep beads followed by Western blotting with the indicated antibodies. α-Tubulin was used as a loading control. (B) The soluble fragment of ACE2-D38E (sACE2-D38E) competed with cell surface ACE2 for CoV-2 S binding in a dose-dependent manner. CoV-2 S-Strep was purified with and immobilized on Strep beads from transfected 293T cells and incubated with lysates from HEK-293A^{ACE2} cells in the absence or presence of various amounts of purified sACE2-D38E-HA (30, 60 μg). Binding of ACE2 to CoV-2 S-Strep beads was examined by Western blotting using the indicated antibodies. (C) sACE2-D38E blocked ACE2 down-regulation by CoV-2 S. HEK-293A^{ACE2} cells were treated with 30 μg of purified CoV-2 S-Strep in the absence or presence of 30 or 60 μg of sACE2-D38E-HA for 6 h. ACE2-Flag levels in the whole cell lysates were analyzed by Western blotting with anti-Flag. (D) sACE2-D38E binds equally well to the S protein from WT and Alpha strains. CoV-2 S-Strep of the WT or Alpha strain was purified with and immobilized on Strep beads from transfected 293T cells and incubated with purified sACE2-D38E-HA. Western blotting was carried out using the indicated antibodies. (E) sACE2-D38E prevented the entry of pseudovirus containing CoV-2 S into cells by neutralizing virus infection. HEK-293A^{ACE2} cells were infected with 1 ml of concentrated pseudovirus expressing VSV-G (left), CoV-2 S (middle), or Alpha S (right) in either the absence or presence of 60 μg of sACE2-D38E-HA or BSA for 6 h. Viral infection and entry were measured by luciferase assays (top panels). ACE2 levels were detected by Western blotting (bottom panels). Data in the graphs in E were derived from at least three independent experiments and are presented as means ± SD by Student's *t* test. $*P < 0.05$.

and is mediated by the clathrin-dependent endocytosis pathway. The μ2 subunit of the AP2 complex binds to the endocytic motif YxxΦ present in the cytoplasmic tail region of ACE2 and through this interaction promotes clathrin-dependent endocytosis, leading to degradation in the lysosome. This ability of ACE2 to bind to the AP2 complex via the cytoplasmic YxxΦ motif has recently been confirmed by a bioinformatic study (Kliche *et al.*, 2021). We speculate that binding of CoV-2 S may result in posttranslational modification of the ACE2 cytoplasmic tail region, allowing the YxxΦ motif to bind to μ2 and recruit clathrin and other endocytic components for endocytosis of ACE2. Alternatively, ACE2 may undergo a constitutive internalization and recycling through its association with the AP2 complex, and CoV-2 S diverts the internalized ACE2 to the lysosomes via altered endosomal sorting.

Both SARS-CoV and SARS-CoV-2 employ the S proteins to engage the ACE2 receptor for cellular entry. Previously, the original SARS-CoV virus has been reported to down-regulate ACE2 via its S protein (Imai *et al.*, 2005; Kuba *et al.*, 2005). However, whether SARS-CoV-2 also causes ACE2 down-regulation was not clear. Here we have demonstrated that SARS-CoV-2 and its variants markedly decrease ACE2 levels in the lung tissue of infected hamsters in vivo. This is consistent with the earlier report that infection of hamsters with a pseudovirus expressing only CoV-2 S resulted in ACE2 down-regulation (Lei *et al.*, 2021b; Yamaguchi *et al.*, 2021) and suggests that CoV-2 S is sufficient for ACE2 down-regulation. Our observation that ACE2 down-regulation occurred within 6 h after infection with SARS-CoV-2, a time frame during which the SARS-CoV-2 virus has not replicated and released viral particles in Caco-2 or Vero E6 cells (Bojkova *et al.*, 2020; Ogando *et al.*, 2020), suggests that viral replication is not required for ACE2 down-regulation. Consistent with this, the inactivated, γ-irradiated virus, which does not express sufficient S protein on the surface (Loveday *et al.*, 2021), failed to down-regulate ACE2. While this paper was being submitted and reviewed, Yamaguchi *et al.* (2021) also reported that SARS-CoV-2 causes lung injury and down-regulates ACE2 in vivo, confirming our findings. SARS-CoV-2 entry into host cells requires sequential

cleavage of the Spike protein upon its binding to ACE2. Either deletion of the furin cleavage site or inhibition of TMPRSS2 significantly reduced SARS-CoV-2 entry and attenuates SARS-CoV-2 pathogenesis (Johnson *et al.*, 2021; Jackson *et al.*, 2022). It would be interesting to investigate whether the spike mutants resistant to cleavage would affect ACE2 levels. Interestingly, we found that CoV-S is more efficient than CoV-2 S in ACE2 down-regulation, probably due to a stronger binding to ACE2, and this seems to correlate with a higher mortality rate of SARS-CoV. HCoV-NL63 S has no significant effect on ACE2 down-regulation, which possibly correlates to its lower pathology (Haga *et al.*, 2008; Glowacka *et al.*, 2010). Several SARS-CoV-2 Spike variants bind to and down-regulate ACE2 with a similar efficiency, yet these variants clearly display different rates of transmission and cause disease of different severities. This suggests that ACE2 down-regulation likely contributes to, but is not fully responsible for, the pathological effects of SARS-CoV-2.

Our comparison of the gene expression profiles between CoV-2 S-treated cells and ACE2 knockdown cells showed only a partial overlap in the set of altered target genes. This could reflect the difference between transient and long-term down-regulation of ACE2 by CoV-2 S and ACE2 knockdown, respectively. In addition, CoV-2 S is likely to affect cellular signaling events through other interacting proteins, such as ZDHHC5 (zinc finger DHHC-type palmitoyltransferase 5) and GOLGA7 (golgin A7) identified in the recent mass-spec study (Gordon *et al.*, 2020). These interactions could also affect the changes in downstream transcriptome. Of note, the overlapped gene set is associated with pulmonary and inflammatory diseases and enriched in cytokine signaling as well as MAPK and JAK-STAT pathways. This is in general agreement with previous global phosphoproteomics analysis and RNA-seq analysis of SARS-CoV-2–infected cells and lung tissues showing that SARS-CoV-2 infection up-regulated innate immune responses with increased cytokine production and type I and II interferon signaling (Winkler *et al.*, 2020), as well as NF-kB, MAPK/p38, and JAK-STAT pathways (Bouhaddou *et al.*, 2020). Thus, ACE2 down-regulation likely contributes significantly to CoV-2 S-induced transcriptional changes and subsequent pathological outcomes.

Down-regulation of ACE2 could also conceivably prevent more viruses from entering the cells after the initial wave of SARS-CoV-2 infection. This could be used by the human tissues and cells as a temporary strategy to block additional viral invasion. Thus, ACE2 down-regulation may temporarily lower viral load and reduce the rate of SARS-CoV-2 infection but may also cause a spectrum of adverse pathological outcomes. Given that binding of CoV-2 S to ACE2 is the key step in SARS-CoV-2 viral entry and the later clinical pathologies, disrupting this binding would be an effective strategy to block viral infection. Indeed, we have developed a soluble ACE2 receptor containing the D38E mutation that displays a stronger binding to CoV-2 S, likely due to a stronger salt bridge between ACE2 and CoV-2 S. Treatment of cells with this soluble receptor markedly reduced viral entry and ACE2 down-regulation. Thus, this soluble fragment could potentially be optimized for therapeutic purposes.

Altogether, our study has uncovered the important mechanism by which SARS-CoV-2 down-regulates ACE2 and demonstrated that this down-regulation can alter cellular signaling pathways involved in SARS-CoV-2–induced lung pathology and inflammatory diseases. These results highlight the importance of blocking Spike protein binding to ACE2 in anti-viral therapy, a strategy further supported and validated by the effectiveness of the soluble sACE2-D38E in reducing CoV-2 S-mediated viral entry and ACE2 down-regulation. Future studies to further optimize the soluble receptor fragments may lead to an effective therapy for clinical management of SARS-CoV-2 infection.

MATERIALS AND METHODS

Request a protocol through *Bio-protocol*.

Plasmids, antibodies, and reagents

The cDNAs encoding SARS-CoV Spike (S), SARS-CoV-2 S, and human ACE2 were purchased from Addgene (#145031, #145780, and #1786). The 2 × Strep-SARS-CoV S-1-1190 and 2 × Strep-SARS-CoV-2 S-1-1208 were generated by PCR and subcloned into the pcDNA3.1 or pRK5M vector. Various SARS-CoV-2 S mutants or variants, ΔRBD (receptor binding domain), D614G, N501Y/D614G, and N501Y/ΔHV69-70/P681H/D614G (Alpha) were generated by PCR and cloned into the pRK5M vector. The sACE2-HA and sACE2-D38E-HA were generated by PCR and subcloned into the pRK5M vector. Human ACE2-Flag and ACE2-GFP were generated by PCR and cloned into the pLVX-IRES-Puro vector kindly provided by Nevan Krogan (University of California, San Francisco). The mCherry-LC3, μ2, Strep-α, mCherry-β2, and HA-isσ2 constructs were generous gifts from James H. Hurley (University of California, Berkeley). The pLVX-μ2-mCherry construct was generated by PCR and cloned into the pLVX-IRES-Hygro vector.

The following antibodies and reagents were obtained commercially: anti-Flag (Sigma; F3165, M2); anti-ACE2 (GeneTex; GTX01160, SN0754); anti-ACE2 (Invitrogen; MA5-32307, SN0754); anti-Spike (GeneTex; GTX632604, 1A9); anti–α-tubulin (Calbiochem; CP06, DM1A); anti-EEA1 (Cell Signaling Technology; 3288T, C45B10); anti-RAB5 (Cell Signaling Technology; 46449T, E6N8S); anti-PDI (Cell Signaling Technology; 3501T, C81H6); anti-AIF (Cell Signaling Technology; 5318T, D39D2); anti-RCAS1 (Cell Signaling Technology; 12290T, D2B6N); anti-LAMP2 (Santa Cruz; sc-18822, H4B4); anti-clathrin heavy chain (Santa Cruz; sc-12734, TD.1); anti-μ2 (Abcam; ab75995, EP2695Y); anti–caveolin-1 (Cell Signaling Technology; 3267T, D46G3); anti-Strep (IBA; 2-1509-001); anti-mCherry (Proteintech; 26765-1-AP); anti-MDM2 (Santa Cruz; sc-56154, HDM2-323); MG132 (Selleckchem; S2619); bafilomycin A1 (Cell Signaling Technology; 54645S), cycloheximide (Sigma; C4859).

Cell culture, transfection, RNA interference, and infection

HEK293T, HEK293A, and A549 cells were cultured in DMEM (Invitrogen) supplemented with 10% fetal bovine serum (FBS) (HyClone) and 50 μg/ml penicillin–streptomycin (Pen-Strep). H1299 cells were cultured in RPMI-1640 (Invitrogen) supplemented with 10% FBS and 50 μg/ml Pen-Strep. Caco2 and Vero cells were cultured in DMEM supplemented with 10% FBS, 1% Non-Essential Amino Acids (Thermo Fisher Scientific), 1% sodium pyruvate (Thermo Fisher Scientific), and 50 μg/ml Pen-Strep. HEK293 GnTI cells were cultured in FreeStyle 293 expression medium (Thermo Fisher Scientific) supplemented with 1% FBS and 1% antibiotic–antimycotic (Thermo Fisher Scientific). All cell lines have been authenticated at the UC Berkeley Cell Culture Facility by the single-nucleotide polymorphism test.

Transfection of cells with cDNA was performed using polyethylenimine (PEI; Polysciences) or Lipofectamine 2000 (Thermo Fisher Scientific) and with siRNA was carried out using Lipofectamine RNAiMAX (Thermo Fisher Scientific) according to the manufacturer's instructions. The following siRNAs obtained from Dharmacon were used: siGENOME SMARTpool Human MDM2 (M-003279-04-0005), siGENOME SMARTpool Human Clathrin Heavy Chain (M-004001-00-0005), siGENOME SMARTpool Human CAV1 (M-003467-01-0005), siGENOME SMARTpool Human μ2 (M-008170-01-005),

siGENOME SMARTpool Human ACE2 (M-005755-00-0005), and siGENOME Non-Targeting siRNA pool (D-001206-13-05).

Pseudoviruses expressing SARS-CoV-2 S or VSV-G were produced by cotransfection of HEK-293T cells with psPAX2 (Addgene; #12260), pLVX-GFP-IRES-Luciferase, and plasmids encoding Flag-tagged SARS-CoV-2 S or VSV-G. The supernatants were harvested at 48 h posttransfection, passed through a 0.45 μm filter, and concentrated by Lenti-X Concentrator (Takara) according to the manufacturer's instructions. The viral titer was determined by counting the GFP-positive cells after infection with serial diluted viral supernatant for 24 h. For infection of HEK-293A^{ACE2} cells, 2.5×10^4 cells were incubated with the pseudovirus at a multiplicity of infection (MOI) of 12 for 6 or 14 h.

Lentiviruses were prepared in HEK-293T cells by transfection with pLVX-ACE2-Flag-IRES-Puro, pLVX-ACE2-AASA-Flag-IRES-Puro, or pLVX-ACE2-GFP-IRES-Puro and viral packaging constructs. The viral supernatant was collected, filtered, and mixed with 4 μg/ml polybrene (Sigma) before being added to the target cells. HEK-293A, A549, and H1299 cells stably expressing human ACE2-Flag, ACE2-AASA-Flag, or ACE2-GFP were generated by lentiviral infection followed by selection in medium containing puromycin.

Protein expression and purification

Protein expression and purification were performed as described previously (Chang *et al.*, 2019). The recombinant VSV-G, CoV-S, and CoV-2 S and the variant proteins in our study are soluble forms of the proteins with the transmembrane domains removed. Briefly, HEK-293 GnTI cells that had been transfected with plasmids expressing 2 × Strep-tagged VSV-G (amino acids 1–464), SARS-CoV S (amino acids 1–1190), or SARS-CoV-2 S and its variants (amino acids 1–1208) were harvested in the lysis buffer (50 mM HEPES, pH 7.5, 1% Triton X-100, 150 mM NaCl, 1 mM $MgCl_2$, 10% glycerol, and 1 mM dithiothreitol [DTT]) supplemented with protease inhibitors (Roche). The clarified lysates were incubated with Strep-Tactin Superflow beads (IBA) for 3 h at 4°C. The beads were washed extensively with the washing buffer (50 mM HEPES, pH 7.5, 300 mM NaCl, 1 mM $MgCl_2$, and 1 mM DTT), and the Strep-fusion proteins were eluted with 10 mM desthiobiotin (Sigma) in the elution buffer (50 mM HEPES, pH 7.5, 150 mM NaCl, and 1 mM DTT) and concentrated with Amicon Ultra Centrifugal Filters (Millipore).

Strep pull down and immunoblotting

Cell lysates were incubated with Strep-fusion proteins overnight at 4°C, followed by Strep-Tactin Superflow beads for an additional 2 h. Proteins bound to the Strep-Tactin Superflow beads were eluted, resolved by SDS–PAGE, and detected by Western blotting as described previously (Zhu *et al.*, 2016; Lu *et al.*, 2020).

Immunofluorescence staining and live-cell imaging

Cells were seeded on glass coverslips, fixed with 4% paraformaldehyde or methanol, permeabilized with 0.1% Triton X-100 for 10 min, and blocked in 5% FBS in phosphate-buffered saline (PBS). Cells were then incubated with primary antibodies at 4°C overnight, washed, and incubated with fluorophore-conjugated secondary antibodies (Thermo Fisher Scientific) for 1 h at room temperature in the dark. After being washed with PBS, the coverslips were mounted on glass slides using VECTASHIELD Antifade Mounting Medium with 4′,6-Diamidino-2-phenylindole (DAPI; Vector Laboratories). Images were captured using a Zeiss LSM 710 confocal microscope.

For live-cell imaging, HEK-293A cells expressing ACE2-GFP that were seeded on a LabTek chambered slide (Nunc) were incubated with purified SARS-CoV-2 S protein and examined under a Zeiss LSM 880 confocal microscope in an equilibrated observation chamber at 37°C with 5% CO_2. Images were acquired at intervals of 1 min and analyzed with ImageJ.

RNA extraction, reverse transcription, and qRT-PCR

Total RNA was isolated from cells using TRIzol Reagent (Ambion). RNA (1 μg) was converted to (cDNA using the ProtoScript II First Strand cDNA Synthesis Kit (New England Biolabs). The qRT-PCR was performed on a Bio-Rad real-time PCR system (Bio-Rad) using the DyNAmo HS SYBR Green qPCR Kit (Thermo Fisher Scientific). The following primers were used: β-actin, Forward: GCCGACAGGATGCAGAAGGAGATCA, Reverse: AAGCATTTGCGGTGGACGATGGA; ACE2, Forward: TCCGTCTGAATGACAACAGC, Reverse: CACTCCCATCACAACTCCAA.

RNA-seq and bioinformatics analysis

Total RNAs was extracted using TRIzol, and cDNA libraries were prepared using high-quality RNA (RNA integrity number > 7). Three replicates for each group were generated and analyzed. RNA-seq was performed by Novogene as described previously (Lu *et al.*, 2020). The DESeq2 R package was used to identify differential expressed genes between two groups. The *P* values were adjusted using the Benjamini–Hochberg method. Genes with an adjusted $P < 0.05$ and absolute Log2(fold change) > 1 were considered to be significantly differentially expressed. DisGeNET and KEGG enrichment analysis of differential expressed genes were performed, and significant enrichment was defined as those with adjusted $P < 0.05$. The heat map was generated as previously described (Winkler *et al.*, 2020; Zhao *et al.*, 2021). Briefly, gene-expression counts per million (CPM) were Log2 transformed followed by z-score normalization, and the z-score normalized data were used to generate the heat map comparing gene-expression levels using MATLAB, where red indicated elevated expression and blue indicated decreased.

SARS-CoV-2 viruses and culture

SARS-CoV-2 strain nCoV-WA1-2020 (WA1) was provided by the Centers for Disease Control and Prevention (Atlanta, GA). SARS-CoV-2 variant strain ancestral B.1 (D614G) was isolated from patient swabs by the California Department of Public Health (Richmond, CA). Variant strain B.1.351 (Beta) was isolated from patient swabs at Stanford University Hospital, Stanford University (Stanford, CA). Virus propagation for all strains was performed by CalDPH in Vero-86 cells in DMEM supplemented with 5% FBS, 2 mM L-glutamine, 100 U/ml Pen-Strep. No mycoplasma contamination was detected in any of the virus stocks. Infectious titers of second-passage stocks used for infection were determined by median tissue culture infective dose $TCID^{50}$ assay. The virus second-passage stocks were deep sequenced, and the RNA sequences of all the virus stocks used were 100% identical to the corresponding variant sequences deposited in GenBank. For $TCID^{50}$ assays and to prepare infectious inoculum, Vero E6 growth medium was prepared by using the formulation above except with 10% FBS and GlutaMAX (Life Technologies) substituted for L-glutamine.

Infection of hamsters

Eight-week-old, male Syrian golden hamsters (Charles River Laboratories; Strain 049) were anesthetized with isoflurane and intranasally inoculated with 4000 $TCID^{50}$ of virus (WA1, D614G, or Beta) suspended in 50 μl of sterile Vero E6 growth medium or 50 μl of medium alone (mock infection). Animals were monitored and weighed daily. At the indicated time points postinfection, animals were humanely killed, and lung tissues were collected. Right lung lobes were weighed and stored in Vero E6 growth medium at –80°C

until processed for $TCID^{50}$ assay and Western blotting. Left lobes were infused with 10% buffered Formalin (Thermo Fisher) and stored in 10 ml of 10% buffered Formalin at 4°C until further processing for H&E staining.

$TCID^{50}$ assay

Virus titer in lungs was determined by a $TCID^{50}$ assay in Vero E6 cells. Briefly, 10,000 cells per well were plated in 96-well plates and cultured for 24 h at 37°C with 5% CO_2 in Vero E6 growth medium. Right lung lobes in Vero E6 growth medium were thawed and homogenized by bead beating. Homogenates were serial 10-fold diluted in Vero E6 growth medium and added to Vero E6 cells. Unused homogenates were retained and stored at –80°C. Cells were observed for cytopathic effect for 6 d. $TCID^{50}$ results were calculated using the Spearman and Kärber method (LOD 200 $TCID^{50}$/ml) and normalized by lung tissue mass (Lei *et al.*, 2021a). Lung homogenates were thawed, and virus was inactivated by heating samples in sealed tubes (75°C, 30 min). Inactivated materials were incubated with SDS loading buffer and further subjected to Western blotting.

Animal use and biosafety

All procedures involving the use of hamsters were approved in advance by the University of California, Berkeley, Institutional Animal Care and Use Committee (AUP 2020-04-13242). All protocols conform to federal regulations, the National Research Council Guide for the Care and Use of Laboratory Animals, and the Public Health Service Policy on Humane Care and Use of Laboratory Animals. All aspects of the use of viable SARS-CoV-2 virus were approved by the office of Environmental Health and Safety at UC Berkeley before initiation of this study. Work with viable SARS-CoV-2 was performed in an animal biosafety level 3 laboratory.

Statistics and reproducibility

All experiments are representative of at least three independent repeats. Data are presented as mean ± SEM or mean ± SD as indicated in the figure legends. Comparisons among groups were performed using Student's *t* test with GraphPad Prism 8.

ACKNOWLEDGMENTS

We thank James H. Hurley for providing cDNAs of the AP2 complex and Nevan Krogan for the pLVX-IRES-Puro construct; Suifang Mao for technical assistance and helpful advice on immunohistochemistry analysis of lung tissue and imaging; and Qiang Zhou for helpful suggestions and discussions. We are also grateful to the Centers for Disease Control and Prevention (Atlanta, GA), the California Department of Public Health (Richmond, CA), and Catherine Blish, Stanford University School of Medicine, for providing SARS-CoV-2 strains. This study was supported by the COVID-19 Catalyst Fund from the Center for Emerging and Neglected Diseases at UC Berkeley to K.L. and by the Fast Grants, a part of Emergent Ventures, a project of the Mercatus Center at George Mason University, to S.A.S. Y.L. is supported by the Berkeley Scholars program.

REFERENCES

Bojkova D, Klann K, Koch B, Widera M, Krause D, Ciesek S, Cinatl J, Munch C (2020). Proteomics of SARS-CoV-2-infected host cells reveals therapy targets. Nature 583, 469–472.

Bonifacino JS, Traub LM (2003). Signals for sorting of transmembrane proteins to endosomes and lysosomes. Annu Rev Biochem 72, 395–447.

Bouhaddou M, Memon D, Meyer B, White KM, Rezelj VV, Correa Marrero M, Polacco BJ, Melnyk JE, Ulferts S, Kaake RM, *et al.* (2020). The global phosphorylation landscape of SARS-CoV-2 infection. Cell 182, 685–712.e619.

Chang C, Young LN, Morris KL, von Bulow S, Schoneberg J, Yamamoto-Imoto H, Oe Y, Yamamoto K, Nakamura S, Stjepanovic G, *et al.* (2019). Bidirectional control of autophagy by BECN1 BARA domain dynamics. Mol Cell 73, 339–353.e6.

Deshotels MR, Xia H, Sriramula S, Lazartigues E, Filipeanu CM (2014). Angiotensin II mediates angiotensin converting enzyme type 2 internalization and degradation through an angiotensin II type I receptor-dependent mechanism. Hypertension 64, 1368–1375.

Dikic I (2017). Proteasomal and autophagic degradation systems. Annu Rev Biochem 86, 193–224.

Finsterer J, Scorza FA, Scorza CA, Fiorini AC (2021). Extrapulmonary onset manifestations of COVID-19. Clinics (Sao Paulo) 76, e2900.

Garcia-Beltran WF, Lam EC, St Denis K, Nitido AD, Garcia ZH, Hauser BM, Feldman J, Pavlovic MN, Gregory DJ, Poznansky MC, *et al.* (2021). Multiple SARS-CoV-2 variants escape neutralization by vaccine-induced humoral immunity. Cell 184, 2372–2383.e9.

Glowacka I, Bertram S, Herzog P, Pfefferle S, Steffen I, Muench MO, Simmons G, Hofmann H, Kuri T, Weber F, *et al.* (2010). Differential downregulation of ACE2 by the spike proteins of severe acute respiratory syndrome coronavirus and human coronavirus NL63. J Virol 84, 1198–1205.

Gordon DE, Jang GM, Bouhaddou M, Xu J, Obernier K, White KM, O'Meara MJ, Rezelj VV, Guo JZ, Swaney DL, *et al.* (2020). A SARS-CoV-2 protein interaction map reveals targets for drug repurposing. Nature 583, 459–468.

Haga S, Yamamoto N, Nakai-Murakami C, Osawa Y, Tokunaga K, Sata T, Yamamoto N, Sasazuki T, Ishizaka Y (2008). Modulation of TNF-alpha-converting enzyme by the spike protein of SARS-CoV and ACE2 induces TNF-alpha production and facilitates viral entry. Proc Natl Acad Sci USA 105, 7809–7814.

Hamming I, Cooper ME, Haagmans BL, Hooper NM, Korstanje R, Osterhaus AD, Timens W, Turner AJ, Navis G, van Goor H (2007). The emerging role of ACE2 in physiology and disease. J Pathol 212, 1–11.

Harvey WT, Carabelli AM, Jackson B, Gupta RK, Thomson EC, Harrison EM, Ludden C, Reeve R, Rambaut A, Consortium C-GU, *et al.* (2021). SARS-CoV-2 variants, spike mutations and immune escape. Nat Rev Microbiol 19, 409–424.

Hikmet F, Mear L, Edvinsson A, Micke P, Uhlen M, Lindskog C (2020). The protein expression profile of ACE2 in human tissues. Mol Syst Biol 16, e9610.

Hoffmann M, Kleine-Weber H, Schroeder S, Kruger N, Herrler T, Erichsen S, Schiergens TS, Herrler G, Wu NH, Nitsche A, *et al.* (2020). SARS-CoV-2 cell entry depends on ACE2 and TMPRSS2 and is blocked by a clinically proven protease inhibitor. Cell 181, 271–280.e278.

Hou YJ, Chiba S, Halfmann P, Ehre C, Kuroda M, Dinnon KH 3rd, Leist SR, Schafer A, Nakajima N, Takahashi K, *et al.* (2020). SARS-CoV-2 D614G variant exhibits efficient replication ex vivo and transmission in vivo. Science 370, 1464–1468.

Hu B, Guo H, Zhou P, Shi ZL (2021). Characteristics of SARS-CoV-2 and COVID-19. Nat Rev Microbiol 19, 141–154.

Imai Y, Kuba K, Ohto-Nakanishi T, Penninger JM (2010). Angiotensin-converting enzyme 2 (ACE2) in disease pathogenesis. Circ J 74, 405–410.

Imai Y, Kuba K, Rao S, Huan Y, Guo F, Guan B, Yang P, Sarao R, Wada T, Leong-Poi H, *et al.* (2005). Angiotensin-converting enzyme 2 protects from severe acute lung failure. Nature 436, 112–116.

Jackson CB, Farzan M, Chen B, Choe H (2022). Mechanisms of SARS-CoV-2 entry into cells. Nat Rev Mol Cell Biol 23, 3–20.

Jia H, Yue X, Lazartigues E (2020). ACE2 mouse models: a toolbox for cardiovascular and pulmonary research. Nat Commun 11, 5165.

Jiang RD, Liu MQ, Chen Y, Shan C, Zhou YW, Shen XR, Li Q, Zhang L, Zhu Y, Si HR, *et al.* (2020). Pathogenesis of SARS-CoV-2 in transgenic mice expressing human angiotensin-converting enzyme 2. Cell 182, 50–58.e58.

Johnson BA, Xie X, Bailey AL, Kalveram B, Lokugamage KG, Muruato A, Zou J, Zhang X, Juelich T, Smith JK, *et al.* (2021). Loss of furin cleavage site attenuates SARS-CoV-2 pathogenesis. Nature 591, 293–299.

Kaksonen M, Roux A (2018). Mechanisms of clathrin-mediated endocytosis. Nat Rev Mol Cell Biol 19, 313–326.

Kliche J, Kuss H, Ali M, Ivarsson Y (2021). Cytoplasmic short linear motifs in ACE2 and integrin beta3 link SARS-CoV-2 host cell receptors to mediators of endocytosis and autophagy. Sci Signal 14, eabf1117.

Kuba K, Imai Y, Rao S, Gao H, Guo F, Guan B, Huan Y, Yang P, Zhang Y, Deng W, *et al.* (2005). A crucial role of angiotensin converting enzyme 2 (ACE2) in SARS coronavirus-induced lung injury. Nat Med 11, 875–879.

Lan J, Ge J, Yu J, Shan S, Zhou H, Fan S, Zhang Q, Shi X, Wang Q, Zhang L, Wang X (2020). Structure of the SARS-CoV-2 spike receptor-binding domain bound to the ACE2 receptor. Nature 581, 215–220.
Lei C, Yang J, Hu J, Sun X (2021a). On the calculation of $TCID^{50}$ for quantitation of virus infectivity. Virol Sin 36, 141–144.
Lei Y, Zhang J, Schiavon CR, He M, Chen L, Shen H, Zhang Y, Yin Q, Cho Y, Andrade L, *et al.* (2021b). SARS-CoV-2 spike protein impairs endothelial function via downregulation of ACE 2. Circ Res 128, 1323–1326.
Li F, Li W, Farzan M, Harrison SC (2005). Structure of SARS coronavirus spike receptor-binding domain complexed with receptor. Science 309, 1864–1868.
Li Q, Nie J, Wu J, Zhang L, Ding R, Wang H, Zhang Y, Li T, Liu S, Zhang M, *et al.* (2021). SARS-CoV-2 501Y.V2 variants lack higher infectivity but do have immune escape. Cell 184, 2362–2371.e2369.
Li W, Moore MJ, Vasilieva N, Sui J, Wong SK, Berne MA, Somasundaran M, Sullivan JL, Luzuriaga K, Greenough TC, *et al.* (2003). Angiotensin-converting enzyme 2 is a functional receptor for the SARS coronavirus. Nature 426, 450–454.
Liu X, Yang N, Tang J, Liu S, Luo D, Duan Q, Wang X (2014). Downregulation of angiotensin-converting enzyme 2 by the neuraminidase protein of influenza A (H1N1) virus. Virus Res 185, 64–71.
Loveday EK, Hain KS, Kochetkova I, Hedges JF, Robison A, Snyder DT, Brumfield SK, Young MJ, Jutila MA, Chang CB, Taylor MP (2021). Effect of inactivation methods on SARS-CoV-2 virion protein and structure. Viruses 13, 562.
Lu Y, Wu T, Gutman O, Lu H, Zhou Q, Henis YI, Luo K (2020). Phase separation of TAZ compartmentalizes the transcription machinery to promote gene expression. Nat Cell Biol 22, 453–464.
Martin DP, Weaver S, Tegally H, San JE, Shank SD, Wilkinson E, Lucaci AG, Giandhari J, Naidoo S, Pillay Y, *et al.* (2021). The emergence and ongoing convergent evolution of the SARS-CoV-2 N501Y lineages. Cell 184, 5189–5200.e5187.
Mayor S, Pagano RE (2007). Pathways of clathrin-independent endocytosis. Nat Rev Mol Cell Biol 8, 603–612.
McCormick KD, Jacobs JL, Mellors JW (2021). The emerging plasticity of SARS-CoV-2. Science 371, 1306–1308.
Mettlen M, Chen PH, Srinivasan S, Danuser G, Schmid SL (2018). Regulation of clathrin-mediated endocytosis. Annu Rev Biochem 87, 871–896.
Ogando NS, Dalebout TJ, Zevenhoven-Dobbe JC, Limpens R, van der Meer Y, Caly L, Druce J, de Vries JJC, Kikkert M, Barcena M, *et al.* (2020). SARS-coronavirus-2 replication in Vero E6 cells: replication kinetics, rapid adaptation and cytopathology. J Gen Virol 101, 925–940.
Ou X, Liu Y, Lei X, Li P, Mi D, Ren L, Guo L, Guo R, Chen T, Hu J, *et al.* (2020). Characterization of spike glycoprotein of SARS-CoV-2 on virus entry and its immune cross-reactivity with SARS-CoV. Nat Commun 11, 1620.
Peng R, Wu LA, Wang Q, Qi J, Gao GF (2021). Cell entry by SARS-CoV-2. Trends Biochem Sci 46, 848–860.
Perera RM, Zoncu R (2016). The lysosome as a regulatory hub. Annu Rev Cell Dev Biol 32, 223–253.
Plante JA, Liu Y, Liu J, Xia H, Johnson BA, Lokugamage KG, Zhang X, Muruato AE, Zou J, Fontes-Garfias CR, *et al.* (2021). Spike mutation D614G alters SARS-CoV-2 fitness. Nature 592, 116–121.
Santos RAS, Sampaio WO, Alzamora AC, Motta-Santos D, Alenina N, Bader M, Campagnole-Santos MJ (2018). The ACE2/angiotensin-(1-7)/MAS axis of the renin-angiotensin system: focus on angiotensin-(1-7). Physiol Rev 98, 505–553.
Shang J, Ye G, Shi K, Wan Y, Luo C, Aihara H, Geng Q, Auerbach A, Li F (2020). Structural basis of receptor recognition by SARS-CoV-2. Nature 581, 221–224.
Shen H, Zhang J, Wang C, Jain PP, Xiong M, Shi X, Lei Y, Chen S, Yin Q, Thistlethwaite PA, *et al.* (2020). MDM2-mediated ubiquitination of angiotensin-converting enzyme 2 contributes to the development of pulmonary arterial hypertension. Circulation 142, 1190–1204.
Vieira C, Nery L, Martins L, Jabour L, Dias R, Simoes ESAC (2021). Downregulation of membrane-bound angiotensin converting enzyme 2 (ACE2) receptor has a pivotal role in COVID-19 immunopathology. Curr Drug Targets 22, 254–281.
Walls AC, Park YJ, Tortorici MA, Wall A, McGuire AT, Veesler D (2020). Structure, function, and antigenicity of the SARS-CoV-2 spike glycoprotein. Cell 181, 281–292.e6.
Wang Q, Zhang Y, Wu L, Niu S, Song C, Zhang Z, Lu G, Qiao C, Hu Y, Yuen KY, *et al.* (2020). Structural and functional basis of SARS-CoV-2 entry by using human ACE2. Cell 181, 894–904.e899.
Washington NL, Gangavarapu K, Zeller M, Bolze A, Cirulli ET, Schiabor Barrett KM, Larsen BB, Anderson C, White S, Cassens T, *et al.* (2021). Emergence and rapid transmission of SARS-CoV-2 B.1.1.7 in the United States. Cell 184, 2587–2594.e2587.
Winkler ES, Bailey AL, Kafai NM, Nair S, McCune BT, Yu J, Fox JM, Chen RE, Earnest JT, Keeler SP, *et al.* (2020). SARS-CoV-2 infection of human ACE2-transgenic mice causes severe lung inflammation and impaired function. Nat Immunol 21, 1327–1335.
Wrapp D, Wang N, Corbett KS, Goldsmith JA, Hsieh CL, Abiona O, Graham BS, McLellan JS (2020). Cryo-EM structure of the 2019-nCoV spike in the prefusion conformation. Science 367, 1260–1263.
Yamaguchi T, Hoshizaki M, Minato T, Nirasawa S, Asaka MN, Niiyama M, Imai M, Uda A, Chan JF, Takahashi S, *et al.* (2021). ACE2-like carboxypeptidase B38-CAP protects from SARS-CoV-2-induced lung injury. Nat Commun 12, 6791.
Yan R, Zhang Y, Li Y, Xia L, Guo Y, Zhou Q (2020). Structural basis for the recognition of SARS-CoV-2 by full-length human ACE2. Science 367, 1444–1448.
Zhao Y, Li MC, Konate MM, Chen L, Das B, Karlovich C, Williams PM, Evrard YA, Doroshow JH, McShane LM (2021). TPM, FPKM, or normalized counts? A comparative study of quantification measures for the analysis of RNA-seq data from the NCI patient-derived models repository. J Transl Med 19, 269.
Zhou D, Dejnirattisai W, Supasa P, Liu C, Mentzer AJ, Ginn HM, Zhao Y, Duyvesteyn HME, Tuekprakhon A, Nutalai R, *et al.* (2021). Evidence of escape of SARS-CoV-2 variant B.1.351 from natural and vaccine-induced sera. Cell 184, 2348–2361.e2346.
Zhu Q, Le Scolan E, Jahchan N, Ji X, Xu A, Luo K (2016). SnoN antagonizes the hippo kinase complex to promote TAZ signaling during breast carcinogenesis. Dev Cell 37, 399–412.